AIAA JOURNAL
Vol. 33, No. 10, October 1995

Surface Pressure Measurements on a Pitching Swept Wing in a Water Channel

April Patterson*
U.S. Army Corps of Engineers, Portland, Oregon 97208
and
Paul Rymarz† and B. R. Ramaprian‡
Washington State University, Pullman, Washington 99164-2920

This paper presents the results of surface pressure measurements on a swept wing of NACA 0015 profile and a back sweep angle of 15 deg, which was pitched at a uniform angular velocity. The pitching axis was perpendicular to the flow direction so that the experiment simulated the pitch-up maneuver of a fixed-wing aircraft. The experiments were performed in an open-surface water channel. The object of the study was to understand the mechanics of vorticity production and dynamic stall in three-dimensional unsteady flows. The phase-locked pressure data which were obtained at several closely spaced spanwise locations of the wing were used to obtain information on the fluxes of spanwise and chordwise vorticity components, in addition to the usual information on the aerodynamic coefficients. The study showed that the three-dimensional dynamic stall over the slightly swept wing is less catastrophic and more gradual than the two-dimensional process over an unswept wing. Other important effects observed were a spanwise variation of the aerodynamic coefficients and the presence of spanwise periodicity in the production of vorticity following the onset of dynamic stall. The experimental data have been archived and are available to any interested user.

Nomenclature

b = span, measured along z
c = chord length, measured along x
C_p = pressure coefficient
C_l = sectional lift coefficient
C_l^* = reduced lift coefficient, $C_l/\cos^2\Lambda$
C_m = moment coefficient
p = distance of the pitch axis from nose
Re = Reynolds number, $U_0 c/\vartheta$
s = longitudinal surface coordinate
U_0 = freestream velocity
W_x = flux of ω_x
W_z = flux of ω_z
x = coordinate along the freestream
y = coordinate normal to chord
z = coordinate perpendicular to the freestream
α = angle of attack
α^+ = nondimensional pitch rate, $\omega c/U_0$
ϑ = kinematic viscosity
Λ = back sweep angle
ρ = density
ω = angular velocity of pitching
ω_x = axial vorticity
ω_z = spanwise vorticity
$'$ = coordinate system perpendicular to leading edge; see Fig. 1

Introduction

THE unsteady vortex dynamics of an airfoil pitched at a uniform angular velocity about its $c/4$ axis has been studied with interest in recent years. Most of these studies relate to two-dimensional flows. Studies reported on the unsteady aerodynamics of three-dimensional flows have, so far, largely pertained to the flow over delta wings. Some studies have recently been reported on the three-dimensional flow associated with pitching/oscillating rectangular wings of finite aspect ratio.[1–10] These include flow visualization as well as pressure/force measurements.

The three-dimensional flows just mentioned represent extremely complex situations. To understand some of the characteristics of the unsteady, three-dimensional vortex dynamics and flow separation, it will be useful to conduct experiments which represent small departures from two-dimensional flows. In fact, this has been the approach used successfully in the past, to understand steady three-dimensional flows. A very comprehensive study of the pressure and velocity field associated with a pitching two-dimensional NACA 0015 airfoil has been completed at Washington State University, using a water channel specially constructed for this purpose (see Conger and Ramaprian[11,12]). This study has now been extended to the investigation of the flow over a pitching wing of the same profile but with a small back sweep angle of 15 deg. Three dimensionality, characterized by a small crossflow, is introduced into the unsteady flow by pitching this wing about an axis perpendicular to the freestream. This paper presents the results of the first phase of this ongoing program of study. In this phase, phase-locked surface pressure distributions were measured at different spanwise locations on the wing while it was pitched at constant angular velocity. Data have been obtained at a Reynolds number $Re = 130{,}000$ and at four different nondimensional pitching rates in the range $0.037 \le \alpha^+ \le 0.21$. Previous studies[11] on the two-dimensional airfoil (unswept wing) have shown that under these conditions existing in the water channel, the flow mimics very closely the behavior representative of much higher Reynolds numbers ($\sim 10^6$). The pressure data from the swept wing have been used to obtain information on the aerodynamic coefficients and the production of vorticity by pressure gradients in the spanwise and chordwise directions.

Experimental Particulars

Experimental Setup

One of the distinguishing features of the present experiments is the unique design of the wing model. The wing is of NACA 0015 profile with $c' = 0.305$ m and $s' = 0.61$ m, measured perpendicular and parallel to the leading edge, respectively. A schematic of

Presented as Paper 94-2254 at the AIAA 25th Fluid Dynamics Conference, Colorado Springs, CO, June 20–23, 1994; received Aug. 5, 1994; revision received Jan. 17, 1995; accepted for publication Jan. 18, 1995. Copyright © 1995 by April Patterson, Paul Rymarz, and B. R. Ramaprian. Published by the American Institute of Aeronautics and Astronautics, Inc., with permission.

*Mechanical Engineer, Hydroelectric Division Center.
†Graduate Research Assistant, Department of Mechanical and Materials Engineering.
‡Professor, Department of Mechanical and Materials Engineering. Member AIAA.

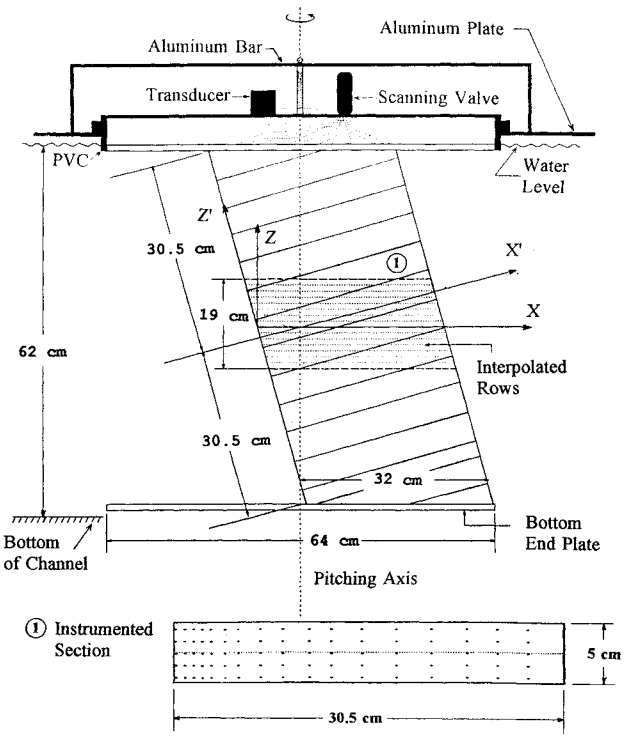

Fig. 1 Schematic of the wing model and experimental setup in the water channel.

the model is shown in Fig. 1. It is constructed in 5-cm-wide airfoil sections of aluminum machined on a numerically controlled milling machine and anodized for corrosion protection. The wing is assembled from these sections, one of which is instrumented with pressure taps. The sections slide on two guide rods such that the instrumented section can be repositioned to varying spanwise locations. This construction allows one to make pressure measurements in several finely spaced spanwise locations without having to provide an impractically large number of pressure taps. The assembled wing has a chord c of 32 cm and a span s of 59 cm. Measurements are reported over the central 19 cm of the span which was found to be free from significant end effects.

The instrumented wing section has a total of 85 pressure taps of 1.25 mm diam arranged in five rows spaced approximately 1 cm apart (see Fig. 1). The pressure taps are unequally spaced along x' and are provided only on one side of the airfoil surface. "Suction" and "pressure" side data are obtained by pitching the airfoil first in the clockwise and then in the counterclockwise direction. With the present design of the model, it is possible to obtain pressure distributions at 22 z' locations at intervals of approximately 1 cm. These data can be used to obtain pressure gradients in the chordwise as well as spanwise directions with acceptable accuracy.

Each end of the wing is fitted with a 1.2-cm-thick Plexiglas® end plate of 64 cm diam. The wing assembly is suspended in the 0.9 m (width) × 0.62 m (water depth) test section of the water channel, as shown schematically in Fig. 1. When mounted in place, the centers of the end plate are located on a vertical axis passing through the $c/4$ point at midspan of the wing. The upper Plexiglas-end plate is bolted into the recess of a PVC pipe which rides on a 64-cm bearing. The bearing is positioned at the center of a rectangular aluminum plate located above the water level. This plate is supported by a large frame (not shown in Fig. 1) independent of the water channel and designed to damp out vibrations generated by the pumps. For more details and a complete description of the water channel, reference may be made to Conger and Ramaprian.[11,12]

Instrumentation

Pitching of the airfoil at constant angular velocity, about the vertical axis through the center of the end plate, is accomplished by a chain attached to the outside of the PVC pipe and driven by a servocontrolled microstepping motor. A digital encoder on the motor shaft provides information on the angular position of the airfoil. The encoder and controller communicate with an IBM-compatible personal computer which also acquires the pressure data.

The pressure measurement system utilizes a diaphragm-type pressure transducer connected between a reference static tap and a surface pressure port via a scanning valve capable of switching among 48 channels. The transducer and scanning valve are carried on an aluminum bar which is mounted on the end plate. A pitot tube immersed in the flow upstream of the wing provides the reference static pressure and stagnation pressure for all experiments. A swivel ball joint mounted above the center of the rotating aluminum bar provides leak-proof communication between the stationary pressure tubing from the pitot tube and the transducer moving with the end plate.

Pressure vs time records were obtained for each pressure tap, one at a time. Steady-flow data were time averaged. The unsteady pressure data were smoothed and corrected for any dynamic response lag effects using a method developed earlier in Conger and Ramaprian.[13] Results were phase averaged over four pitching realizations (which have been shown in Ref. 11 to be repeatable, at prestall incidences, within ±4.3% in C_p) as a reasonable compromise between accuracy and experimental time. Phase-locked pressure distributions on the airfoil were later obtained from these individual pressure vs time (angle) records.

Experimental Conditions

As already mentioned, all of the measurements reported in this paper were made at a Reynolds number of 130,000. Data were obtained at four different pitching rates, $\alpha^+ = 0.037, 0.075, 0.104$, and 0.207. Measurements were made at 22 z' locations extending over about 22 cm. These data were subsequently interpolated to obtain pressure distributions C_p vs x/c and C_p vs s/c at 19 spanwise locations (i.e., z direction) extending over a distance of 19 cm. These pressure data were integrated to obtain the lift, pressure–drag, and moment about the pitching axis, following standard procedure (see, for example, Ref. 7). The details of calculation are described in Patterson.[14] Pressure gradients along the x' and z' directions were computed from the original 22 sets of data. These results were subsequently used to evaluate the pressure gradients (or, equivalently, the vorticity fluxes) in the x and z directions. The experimental uncertainties are estimated to be 6% for C_p and the aerodynamic coefficients and ±0.07 deg for α. The surface vorticity fluxes (or, equivalently, the surface pressure gradients) obtained from smoothed, phase-locked surface pressure distributions are estimated to be accurate to within 12%.

Results and Discussion

Steady Flow

Generally, spanwise flow near the wing surface tends to convect end effects to the midspan region of the wing. It is, therefore, necessary in principle to use much larger aspect ratios for the swept wing than for unswept wing, if end effects are to be kept small. Considerations of the physical limitations of the flow facility and a desire to use a large chord (to obtain more favorable Reynolds number, angular velocity of pitching, and spatial resolution of pressure and velocity data), however, dictated the use of a relatively small aspect ratio and restriction of the study to a small (but significant) spanwise region around the midspan plane. The steady-flow data were used to assess the effect of the proximity to the end, on the uniformity of the flow conditions over this region of study. It was found from the C_p vs x' distributions measured at different z' locations over the stationary wing that, typically, the overall variations in C_p along z' were on the order of ±0.1 at an incidence of 14 deg in the region $-0.33 < z'/c' < +0.33$. The lift curves for three spanwise locations shown in Fig. 2a also confirm that there is no significant spanwise variation in lift. This indicates that the spanwise region of interest can be regarded as being acceptably far away from the ends, at least so long as the flow is not significantly detached from the surface. Flow visualization studies conducted using dyes of different color (discussed in Rymarz[15]) also supported this observation. Since it is not easy to distinguish "end effects" from the imposed three-dimensional effects in the case of the pitching wing, we can only extrapolate from the steady-flow experiments and assume that, even over the pitching wing, the end effects are not significant over this

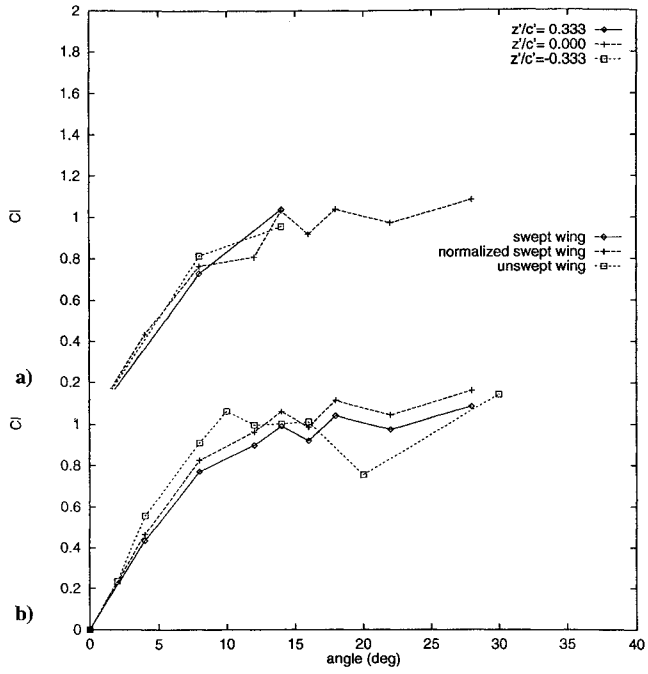

Fig. 2 Lift data for the stationary wing: a) results for different spanwise locations and b) comparison with unswept-wing data from Ref. 8. Normalized results in b) correspond to C_l^*.

spanwise region so long as the flow is not massively separated from the surface, i.e., almost close to the occurrence of dynamic stall. It should be noted, however, that end effects may become significant after separation both in steady and unsteady flow. The present results for the pitching wing at post-dynamic-stall incidences are, therefore, to be interpreted with some care.

Also, in view of the small variation of pressure in the spanwise direction, it is reasonable to use the span-averaged C_p vs x'/c' distribution to represent the steady-state results. Since $x/c = x'/c'$, this average C_p vs x'/c' distribution, when transformed to the freestream (x, y, z) coordinate system, yields an identical C_p vs x/c distribution. The lift curve obtained from the averaged C_p vs x/c distribution is shown in Fig. 2b and compared with the results for an unswept wing from Conger and Ramaprian.[11] It can be seen that sweep results in a reduction of the lift coefficient. Also, the swept wing does not exhibit a drastic drop in lift beyond stall. This latter result is due to the presence of a spanwise component of velocity which causes the onset of separation to be gradual rather than catastrophic. With regard to the lift data at prestall incidences for the swept wing, it has been shown (see, for example, Lorber et al.[5]) that a "reduced" lift coefficient C_l^* defined by normalizing the lift by $1/2\rho U_0^2 \cos^2 \Lambda$ better collapses the lift curves for the swept and unswept wings. The results of this normalization is also shown in Fig. 2b. It is seen that this normalization does not result in a complete collapse of the swept and unswept wing data, although the results are brought closer together. The residual discrepancy may be attributed to Reynolds number effects. In the two-dimensional experiments of Conger and Ramaprian,[11] early laminar–turbulent transition seems to have occurred in the boundary layer over the leading-edge region of the wing surface, even at the moderate experimental Reynolds number of 1.3×10^5. The early triggering of transition was attributed in Ref. 11 to the high-freestream turbulence of about 1% in the water channel. The early transition would result either in the total elimination of the so-called leading-edge separation bubble (characteristic of low-Reynolds number flows over airfoils) or in the formation of a very small bubble, thereby producing larger lift coefficients characteristic of flows at much higher Reynolds numbers. Apparently, such early transition and consequent "simulation" of high-Reynolds number effects did not occur at the Reynolds number of 1.3×10^5 in the present steady-flow experiments over the swept wing, in spite of the high-freestream turbulence. This is presumably because of the presence of the spanwise flow, which is known to delay transition. The resulting formation of a separation bubble would explain the observed reduction in lift relative to the unswept wing. The presence of a small separation bubble could, in fact, be inferred from a mild plateau observable in the pressure distribution curves for the steady swept wing, shown in Patterson.[14] However, the introduction of unsteadiness in to the flow changes the entire dynamics as will be seen from the corresponding results for the pitching wing, which are presented next.

Unsteady Flow

Phase-locked pressure data for the pitch-up maneuver will be presented in the x–z coordinate plane. Note that the location of the pitch axis with respect to the leading edge varies with z, thus introducing three dimensionality and, hence, spanwise variation in the unsteady flow. In fact, based on the observations in steady flow, we believe that all systematic spanwise variations of flow properties observed in the unsteady flow are almost entirely due to the pitch-axis geometry and not significantly due to end effects. A typical experimental condition of $\alpha^+ = 0.075$ is used for a detailed presentation of results. Effects of nondimensional pitch rate are then explored with $\alpha^+ = 0.037$, 0.104, and 0.207.

Surface Pressure

A typical set of suction side pressure-angle traces is presented in Fig. 3. The traces for different s/c locations are offset vertically for the sake of clarity. A three-dimensional plot of the pressure-angle history for all s/c values is shown typically for the midspan plane $z/c = 0$ in Fig. 4. It is seen that over most of the pressure side ($s/c < 0$) except near the nose, no significant changes occur in C_p during the pitching process. However, large variations occur on the suction side. Specifically, the suction pressure exhibits a steady increase in magnitude with incidence, leading to the appearance of

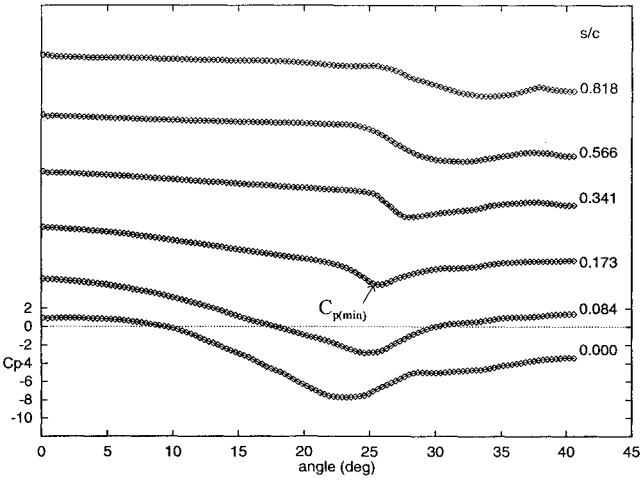

Fig. 3 Typical pressure-angle traces at selected pressure tap locations: $z/c = 0$ and $\alpha^+ = 0.075$.

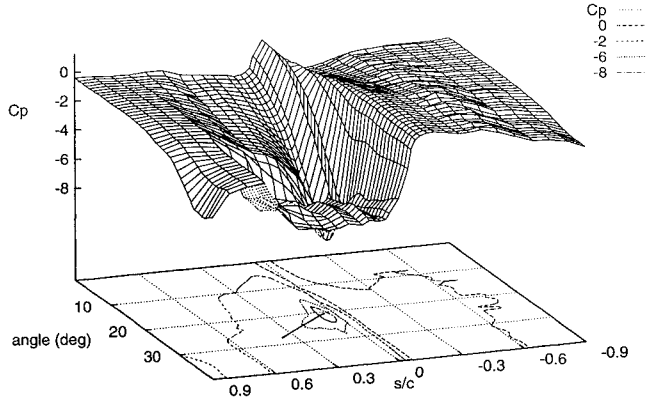

Fig. 4 Three-dimensional plots of pressure-angle history; $z/c = 0$, $\alpha^+ = 0.075$; lower plot, C_p contours; solid line in contour map indicates the locus of α_{min} in the s/c–α plane.

a local pressure minimum at some incidence, beyond which it begins to decrease. At the nose, $C_{p(\min)}$ has a magnitude of about 9 and occurs at an incidence of about 23 deg. The pressure minima grow weaker and occur later during pitch up, at the more downstream locations, as is clearly seen from Fig. 3. The behavior of these pressure-angle traces is qualitatively similar to that observed in the case of unswept wings.[11]

The occurrence of $C_{p(\min)}$ has been usually associated with the formation/arrival of the leading-edge vortex at the particular location. The chordwise movement of $C_{p(\min)}$ can, therefore, be related to the convection of the leading-edge vortex, as has been done in Lorber[6] and Green et al.[16] In the present studies, the angle $\alpha_{\min}$ at which the local pressure minimum occurs at each chordwise location (s/c) was obtained from the pressure-angle records. The variation of $\alpha_{\min}$ with s/c at the midspan plane, during the period from $\alpha \approx 22$ deg (when the vortex first appears on the wing) to $\alpha \approx 28$ deg (approximate incidence for maximum lift) is shown by the solid line drawn on the pressure contour map displayed at the bottom of Fig. 4. It was found that this curve can be approximated by a straight line, the slope of which gives the convection velocity of the suction maximum point in the chordwise direction, as $0.17U_0$. A similar result was obtained for all spanwise locations. This value can be compared with $0.25U_0$ and $0.09U_0$ reported for the inboard and tip region, respectively, of a rectangular wing in Ref. 4.

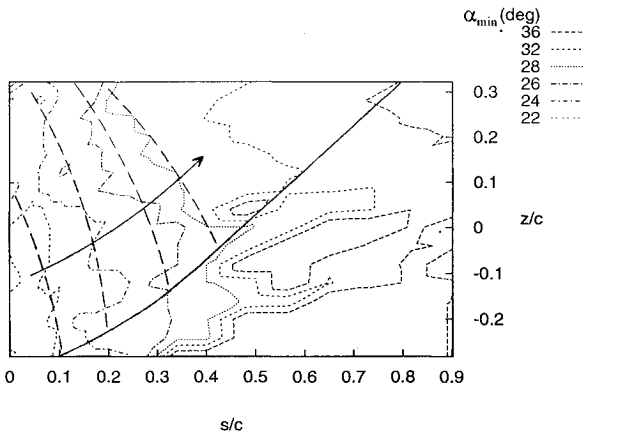

Fig. 5 Lines of constant $\alpha_{\min}$ in the s–z plane, $\alpha^+ = 0.075$: broken lines, location of the average $C_{p(\min)}$ front at different incidences; arrow, the direction of front motion; and solid line, limit to the left of which pressure minima can be identified.

From the $\alpha_{\min}$ vs s/c results obtained at different spanwise locations, it is possible to draw the contours of $\alpha_{\min}$ in the s–z plane, in the range of 22–36 deg. These contours are shown in Fig. 5. The contour for each $\alpha_{\min}$ in this figure represents the line on the wing surface on which $C_{p(\min)}$ (and, hence, the dynamic stall vortex) first appears at that incidence. Hence, each contour line can be regarded as the signature of the instantaneous axis (or a "wave front") of the stall vortex on the surface of the wing. The contour lines have a jagged appearance which is due to the uncertainty in the determination of $\alpha_{\min}$ from the pressure-angle traces. However, it is still possible to observe two overriding trends. These are as follows.

1) $C_{p(\min)}$ moves along the wing surface, as indicated by the arrow in Fig. 5, with a generally oblique wave front shown by the bold dashed line for each incidence. More specifically, $C_{p(\min)}$ first occurs at the lower spanwise positions ($z/c < 0$) and spreads upwards ($z/c > 0$) during pitching.

2) This average wave front is modulated by what appears to be spanwise periodicity which is evident over the background noise.

These results bear qualitative resemblance to the observations of Lorber[6] in his studies of unsteady flow near the tip of a rectangular wing. However, no spanwise waviness was apparent in his data. It should be noted though that the two flows are not similar, even though they are both three dimensional. Whereas the baseline steady flow near a wing tip is three dimensional, three-dimensional unsteadiness is imposed in the present case (via the geometry of the pitching axis) on what is essentially a quasi-two-dimensional steady baseline flow.

The movement of the wave front in Fig. 5 can, however, be identified only up to a certain incidence, beyond which it gets blurred. The solid line drawn across Fig. 5 approximately represents this limiting line in the s–z plane, to the left of which the contour lines can be distinguished. Thus, pressure minima can be identified only up to an incidence of about 22 deg (and $s/c \approx 0.1$) at $z/c = -0.3$, whereas they can be identified even up to 36 deg (and $s/c \approx 0.8$) at $z/c = +0.3$. It will be seen later that these angles approximately represent the incidence for maximum sectional lift at each spanwise position. The issue of spanwise modulation will be discussed later.

Figure 6 shows typical phase-locked pressure distributions in the midspan plane at three selected instantaneous angles of attack. The suction peak (the maximum magnitude of the phase-locked prefssure) increases with increasing incidence and is located within 5% of the nose up to the stall angle. The suction peak reaches a maximum at 22.24 deg in this case, after which it collapses. A slight bulge also appears just downstream of the suction peak at this incidence. It then develops to an approximate constant-pressure plateau, and the suction side curve distorts to that seen at 26.31 deg. The figure

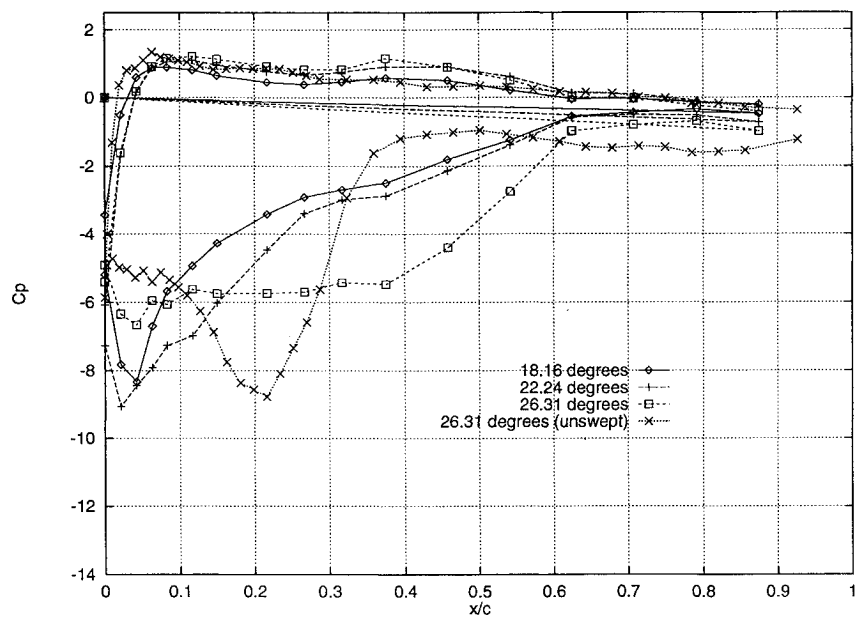

Fig. 6 Typical phase-locked distributions at different incidences; $z/c = 0$, $\alpha^+ = 0.075$; unswept-wing data from Ref. 8.

also shows corresponding results at the same angle of incidence for an unswept wing. The appearance of the long plateau (with a barely noticeable mild hump) in the pressure distribution for the unswept wing is a contrast from a sharper second suction peak observed in the case of the unswept wing. However, like the second suction peak in the latter case, the appearance of the plateau indicates the presence of a stall vortex, which is eventually to be followed by the occurrence of $C_{l\max}$ and dynamic stall. The difference in the pressure distributions observed prior to the onset of dynamic stall in the two cases is due to the difference in the nature of boundary-layer separation in the two cases. In the two-dimensional unsteady flow over the unswept wing, separation is catastrophic with the shear layer being ejected from the surface in the form of a compact and well-defined stall vortex. In the three-dimensional flow over the swept wing, separation occurs more gradually, resulting in a less well-defined, stretched-out dynamic stall vortex.

Aerodynamic Coefficients

The effects of sweep and unsteadiness on the coefficients of lift and pitching moment are shown in Figs. 7a and 7b by comparing the present data with those at the same Reynolds number from Conger and Ramaprian,[11] for the unswept wing pitched at nearly the same rate ($\alpha^+ = 0.072$) about its $c/4$ axis. To eliminate the effect of pitch axis location, swept-wing results at midspan ($z/c = 0.000$) where the pitch axis is located at $c/4$, are used for comparison. Also presented for comparison are the present steady-flow swept-wing data. Note that the data have not been corrected for blockage effects. The unsteady lift curve for the swept wing departs from the steady lift curve at $\alpha \approx 8$ deg and continues to increase nearly with the same slope up to an incidence of about 25 deg. Beyond this incidence, the lift curve flattens out and reaches a maximum value of about 3.5 at an incidence of about 27 deg after which the lift begins to decrease gradually due to the occurrence of dynamic stall. The lift data for the swept and unswept wings coincide up to an incidence of about 10 deg beyond which the swept wing seems to produce a slightly higher lift. This trend continues until dynamic stall occurs with the swept wing displaying maximum lift at a slightly larger incidence. Note that the larger maximum lift associated with the second peak in the unswept-wing data in Fig. 7 is suspected to be caused by blockage effects (see Ref. 11 for a discussion on the blockage effects) and, hence, is likely to be spurious. The smaller size of the model and three-dimensional features of the flow resulted in smaller blockage effects (estimated to be less than 18% at an incidence of 30 deg) in the present case. Once again, as in steady flow, the more gradual decrease in lift at poststall incidences, in the case of the swept wing, is a result of the less catastrophic nature of separation.

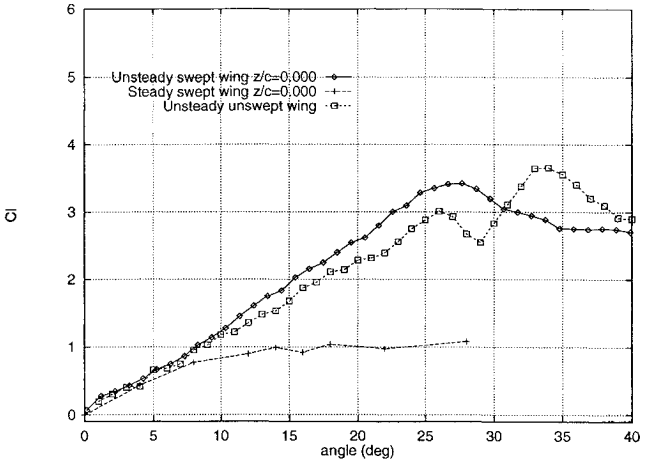

a)

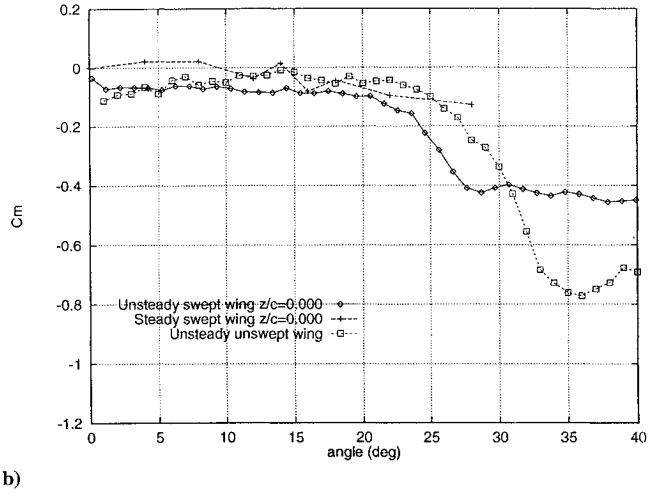

b)

Fig. 7 Lift and moment coefficient comparisons; $\alpha^+ = 0.075$; unswept wing data are from Ref. 8.

The closer behavior of the swept and unswept wings in the prestall region of unsteady flow (which is in contrast to the relatively lower lift slope observed for the swept wing in steady flow in Fig. 2b) is attributed to the occurrence of (similar) early transition (resulting in the elimination/attenuation of the separation bubble) in both cases. The combination of imposed unsteadiness and high-freestream turbulence is apparently adequate to trigger early transition over the swept wing even in the presence of the spanwise flow. The elimination/attenuation of the separation bubble leads to "simulation" of high-Reynolds number behavior and, hence, comparable lift characteristics for the swept and unswept wings in unsteady flow.

The results for drag coefficient, obtained from integration of the pressure distribution over the wing, showed little effect of sweep even up to the incidence of maximum lift. Beyond this, the swept-wing drag was found to increase more gradually and remained less than for the unswept wing even at large incidences. These results are not presented here for the sake of brevity. They are described in detail in Ref. 14.

Figure 7b shows results for the coefficient of pitching moment about the pitching axis. These results also show that there is very little effect of sweep on the pitching moment up to an incidence of about 10 deg. Beyond that incidence, sweep slightly increases the magnitude of the negative pitching moment. Both swept and unswept wings exhibit an increase in pitching moment in unsteady flow at large poststatic stall incidences. The swept wing experiences an earlier and larger increase in pitching moment, but this increase beyond dynamic stall is not catastrophic. In fact, $C_{m\max}$ is significantly smaller for the swept wing. All of these effects on the aerodynamic coefficients can be explained as being due to a less catastrophic modification in flow pattern accompanying a nonsingular, open-type of separation. Past studies of steady flows (e.g., Wang[17]) have identified this type of separation in three-dimensional flows.

Spanwise Variations

The three-dimensional plots in Figs. 8a and 8b show the variations in C_l and C_m with incidence and spanwise location. There is no significant spanwise variation in C_l at incidences less than about 20 deg, as can be seen from contour lines which are nearly parallel to the z axis (except for the blips seen at $z/c \approx 0.1$, which are suspected to be due to experimental errors). After the appearance of the stall vortex, however, spanwise variation becomes noticeable. The trend that is most clearly seen is an increase in $C_{l\max}$ and a delay in the occurrence of $C_{l\max}$ as z/c increases from the bottom ($z/c = -0.322$) to the top ($z/c = +0.322$) of the wing, as shown by the maximum-lift line (solid line) drawn on the contour map at the bottom of Fig. 8a. A similar trend in spanwise variation, namely larger values and delayed occurrence toward the top of the wing, was seen in the drag data also (see Ref. 14 for details).

The increasing moment arm lengths from bottom to top of the wing contribute to a larger and even more ordered spanwise variation in C_m about the pitch axis. An increase in the magnitude of the pitching moment accompanied by increasing negative slope toward the bottom of the wing is evident in Fig. 8b, even at prestall angles. Also the increase in the magnitude appears at earlier incidences toward the bottom of the wing.

Figures 7 and 8 very clearly show that the dynamic stall process over the swept wing is significantly different from that over the unswept wing. Furthermore, this difference is not merely a quasi-two-dimensional pitch-axis effect, as can be seen from the noncatastrophic behavior of the aerodynamic coefficients (especially C_m) at postdynamic stall incidences in the former case. It is, therefore, reasonable to conclude that even a small sweep can produce significant three-dimensional effects in the case of a pitching wing.

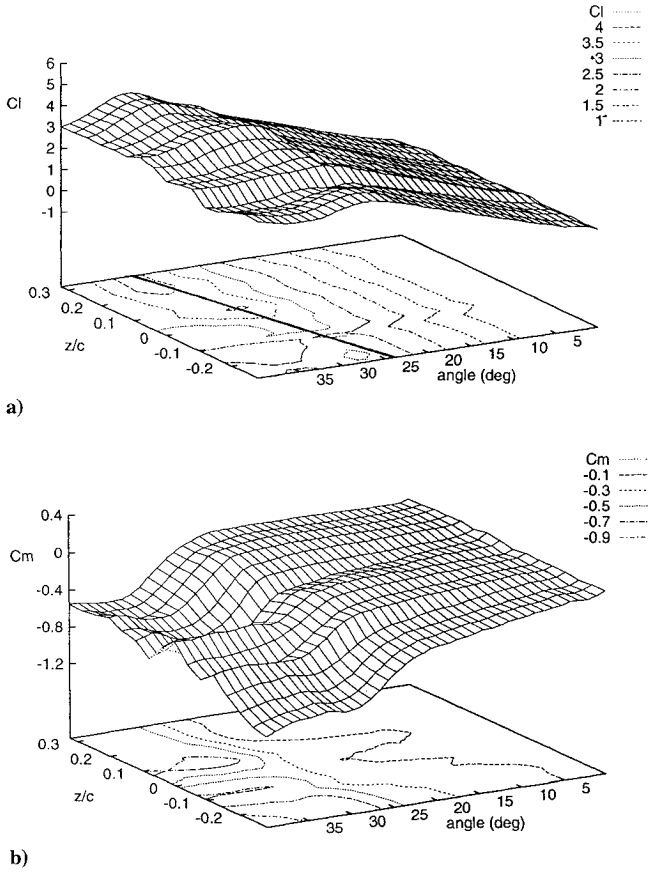

Fig. 8 Variation of sectional lift and sectional pitching moment with incidence and spanwise location; $\alpha^+ = 0.075$.

Pitch Rate Effects

Data obtained at different pitch rates showed that the pressure distributions are qualitatively similar to those obtained at $\alpha^+ = 0.075$. However, suction peaks were larger and occurred at higher angles of incidence as the pitch rate was increased. The detailed pressure distributions at all of the pitch rates studied are presented in Ref. 14. Only the corresponding aerodynamic coefficients C_l and C_m are shown here, typically for the midspan location, in Figs. 9 and 10. Note that these results are plotted in terms of an effective angle of attack α_{eff} defined on the basis of the relative freestream velocity vector at the nose of the pitching wing. It can be easily shown that this effective angle is given by the equation

$$\alpha_{\text{eff}} = \alpha - \alpha^+(p/c)\cos\alpha \tag{1}$$

The use of α_{eff} serves to minimize, even if not eliminate, the effect of the change in the relative orientation of the incident velocity vector with pitch rate. It can be seen from the figure that an increase in pitch rate, especially at the lower pitch rates, primarily results in higher $C_{l\,\max}$ values at increasing incidence. This also means that the occurrence of dynamic stall is delayed at higher pitch rates. In fact, at the highest pitch rate studied ($\alpha^+ = 0.204$), dynamic stall did not occur within the range of incidence studied. An important feature to note is that, except at the highest pitch rate studied, the lift slope is not significantly affected by pitch rate until the flow is close to dynamic stall. Some reduction in the slope is, however, observed at the highest pitch rate. The higher lifts realized at prestall incidences at moderate pitch rates ($\alpha \leq 0.1$), thus, appear to be essentially a quasisteady (and nearly inviscid) effect resulting from wall motion (which tends to keep the boundary layer attached to the wall up to larger incidences) rather than a direct unsteady effect. This is the same conclusion as was reached in Ref. 11 for the unswept wing. Once the stall vortex begins to form, however, its growth, convection, and shedding are no longer either quasisteady or inviscid.

Figure 10 shows that pitching moment coefficients for different pitch rates also overlap at incidences below the incidence corresponding to the onset of the stall vortex (i.e., the appearance of the pressure plateau in Fig. 6) but increase, in general, with pitch rate at higher incidences. The drag coefficient (not shown here) was found to exhibit a similar trend. It may be noted that the large increase in the magnitude of C_m occurs earlier than the appearance of $C_{l\,\max}$, i.e., considerably earlier than the occurrence of dynamic stall. The dynamic effect on C_m is, thus, more significant than on C_l.

The results obtained at other spanwise locations at the aforementioned pitch rates were found to be qualitatively similar to those observed at midspan. The spanwise variations of the aerodynamic

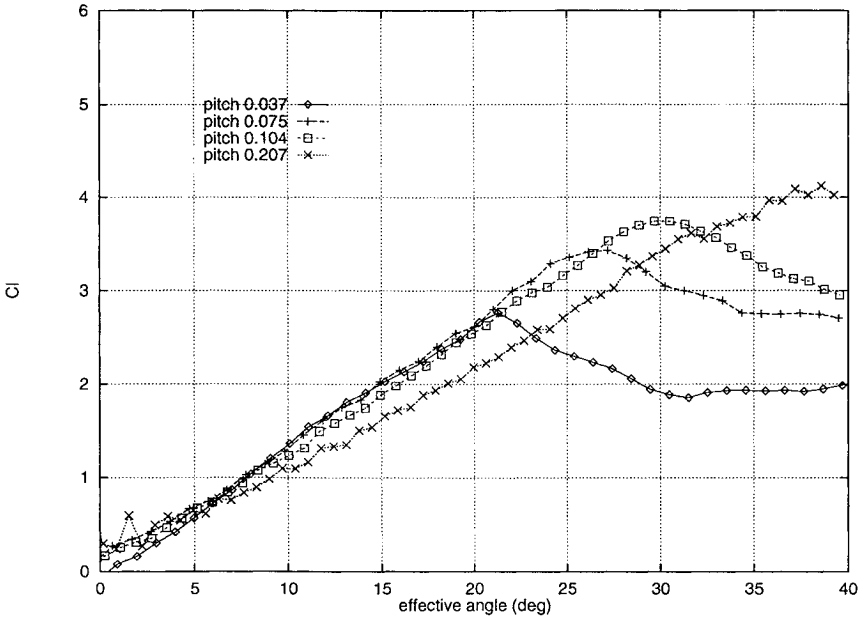

Fig. 9 Effect of pitch rate on lift; $z/c = 0$.

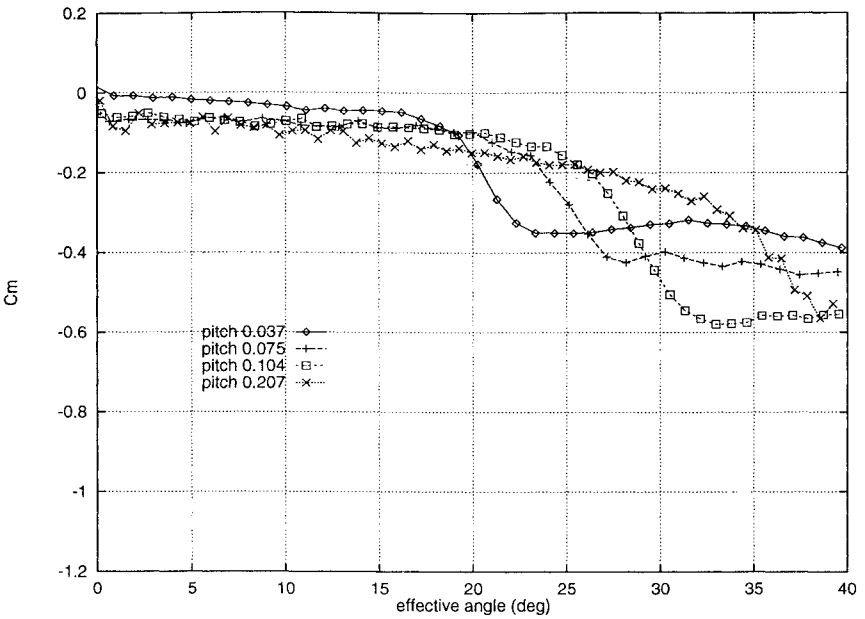

Fig. 10 Effect of pitch rate on pitching moment; $z/c = 0$.

coefficients at the different pitch rates were qualitatively similar to those described for $\alpha+ = 0.075$ and were found to be significant only beyond the incidence corresponding to the inception of the stall vortex, i.e., at progressively larger incidences at higher pitch rates. In fact, there was little spanwise variation in the lift coefficient at the highest pitch rate of $\alpha+ = 0.204$, at which dynamic stall was not observed at all within the incidence range studied. On the other hand, spanwise variations in drag and pitching moment, which occurred earlier than the onset of the stall vortex, were observed at all pitch rates. See Ref. 14 for details of the results at the higher pitch rates.

Vorticity Fluxes

It can be shown (see Panton[18]) that at the wing surface the Navier–Stokes equations reduce to the following form:

$$\frac{\partial C_p}{\partial(s/c)} = -\frac{\nu c}{U_0^2}\frac{\partial \omega_z}{\partial y} = W_z \tag{2}$$

and

$$\frac{\partial C_p}{\partial(z/c)} = \frac{\nu c}{U_0^2}\frac{\partial \omega_x}{\partial y} = -W_x \tag{3}$$

Thus, the nondimensional pressure gradients in the spanwise and chordwise directions represent the nondimensional surface fluxes $(-W_x)$ and W_z of the chordwise and spanwise vorticity components ω_x and ω_z, respectively. These typical fluxes were evaluated and are shown for the suction side of the wing in Figs. 11a–11f, for $\alpha^+ = 0.075$ and, in each case, for three angles of incidence. The three-dimensional plots are drawn at a view angle such that the aft region of the wing (where W_x is negative and W_z is positive) is brought into view. This is the region where interesting features of three dimensionality are observed. Note that negative values of W_z represent the infusement of negative (lift-producing) spanwise vorticity ω_z from the surface in to the flow. Large negative values of W_z occur very near the leading edge. Some of this can be seen around $s/c = 0$ in Figs. 11a–11c, even though the maximum negative value (≈ -180 units) which occurs at a slightly negative value of s/c is off the scale and, hence, not seen in the figures. At the more downstream locations in these figures, humps can be observed. The most upstream hump in each case corresponds to the plateau (or a mild second suction maximum) typically seen in Fig. 6. It represents the stall vortex still staying very close to the surface. It is seen that the hump appears first at the lowest spanwise location and is seen at upper spanwise planes as the angle of incidence increases from 24 to 28 deg. The hump gets elongated with time and also appears to break into longitudinal subhumps. The subhumps in the longitudinal direction most likely represent signatures of the vortices arising from the instability of the shear layer separating from the surface during the early stages of the dynamic stall vortex evolution. The interaction of these vortices with the surface results in the wavy pressure distribution along the flow direction.

At 28-deg incidence, the stall vortex (identified by the modulated hump) is seen to be occupying the entire chord length of the wing at the lowest plane whereas it occupies only about half the chord length of the wing at the uppermost plane. Thus, one can conclude that the stall vortex structure propagates obliquely across the wing surface in a wavelike manner. The vortex is also oriented obliquely to the flow direction. The preceding statements refer to the average structure of the stall vortex. However, Figs. 11a–11c also show that there is significant spanwise modulation of this structure and that this modulation is fairly periodic. Figures 11d–11f show the distributions of the flux $-W_x$, which essentially lead to the same conclusions, both with respect to the propagation of the vortex with an oblique wave front and with respect to the spanwise periodicity. Figures 11a–11f complement Fig. 5, which shows spanwise periodicity in the contours of $\alpha_{\min}$. Some evidence of this periodicity can also be seen in the poststall distributions in Fig. 8. The precise cause of this periodicity is not known. One speculation is that this periodicity is the result of some Taylor–Gortler type instability produced by the concavity of the streamlines over the suction side of the wing, especially under poststall conditions. Unfortunately, poststall pressure data in this spanwise detail are available only for the pitching swept wing and not for other cases, such as stationary/pitching unswept wing or stationary swept wing. It is not, therefore, clear whether this periodicity is peculiar to the pitching swept wing, or is a general feature of all separating boundary layers over wing surfaces. It is also not clear whether and how a change in the aspect ratio of the wing will affect this periodicity. Further studies are clearly needed to understand this aspect of the flow.

Figures 12a–12c show a vector plot of the vorticity flux vector at the surface. The wing is shown in the swept-back position, and the individual vectors shown correspond to data from the 22 rows of individual pressure taps in the region $0.17 < s'/c' < 1.0$ and $-0.33 < z'/c' < 0.33$. The direction of the arrows indicate the direction of the vorticity vector infused at the surface, and the length of the arrow denotes the magnitude of its surface flux (or the pressure gradient). The figures correspond to the same incidences as in Fig. 11. Once again, the region $s/c < 0.17$ where the fluxes are very large is excluded from the figure in order that the interesting behavior of the flux vectors in the downstream region can be scaled and presented more clearly. Note that the vorticity vector

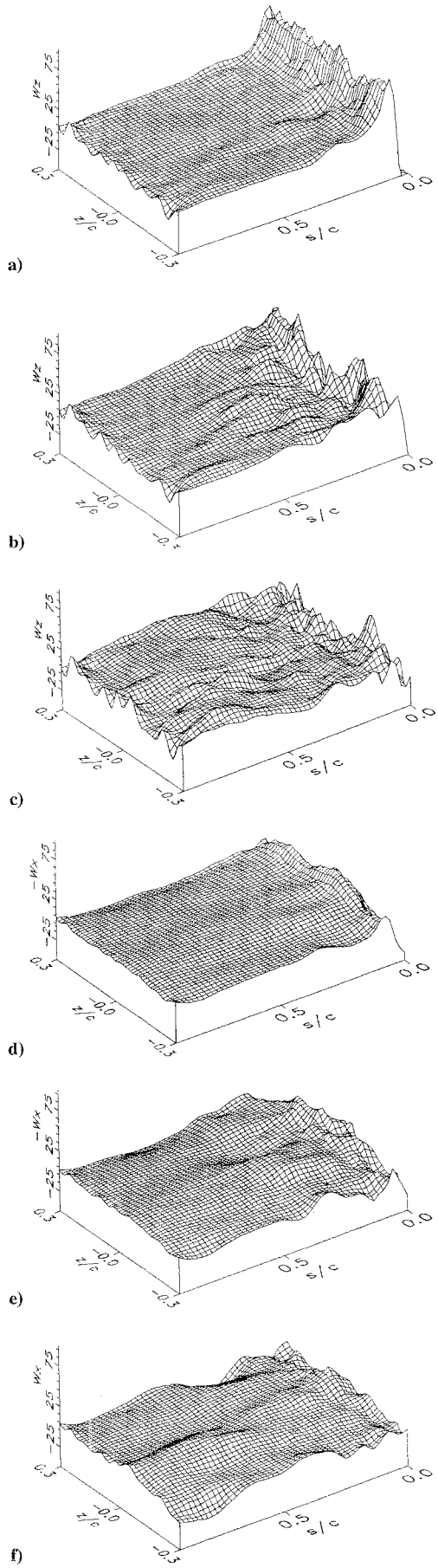

Fig. 11 Vorticity fluxes W_z and W_x at the wing surface caused by pressure gradients in the x and z directions; $\alpha^+ = 0.075$: a) W_z, $\alpha = 20$ deg, b) W_z, $\alpha = 24$ deg, c) W_z, $\alpha = 28$ deg, d) W_x, $\alpha = 20$ deg, e) W_x, $\alpha = 24$ deg, and f) W_x, $\alpha = 28$ deg.

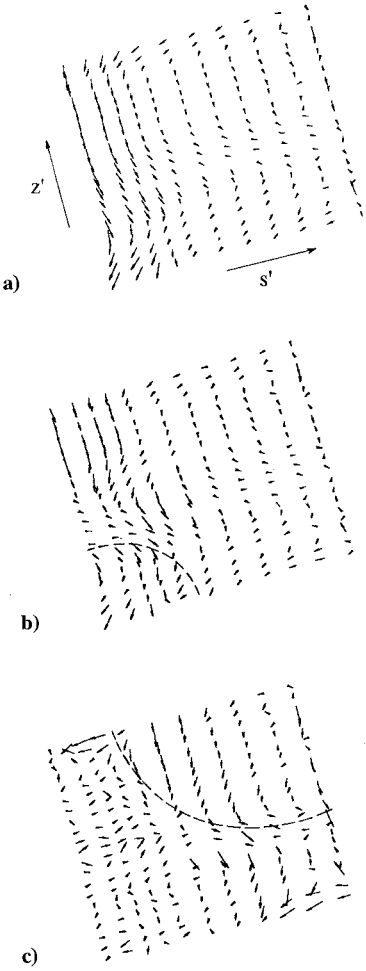

Fig. 12 Vorticity flux vectors at the wing surface corresponding to the conditions in Fig. 11.

generated at the surface is perpendicular to the pressure gradient vector.

At a low incidence of 20 deg, the flux vectors appear to be organized and, in fact, exhibit a spanwise periodicity. At 24 deg, the stall vortex begins to appear near the bottom left corner. This results in the flux vectors (or the pressure field) getting disorganized slightly in that region of the wing. The structure over the rest of the wing is undisturbed, indicating that there is no influence of the stall vortex on the global pressure field. At 28 deg, the stall vortex has spread over a substantial part (southwestern-half) of the wing, as seen from Fig. 12c. However, flow structure in the remaining part of the wing still appears to be organized and periodic. This shows that the vortex has not lifted off the surface, which would have resulted in massive stall. In fact, there was no evidence of such massive stall occurring in the flow even at higher incidences. This was also confirmed from flow visualization studies. The gradual, rather than a catastrophic, drop in lift and pitching moment at poststall incidences is also consistent with this observation. The evolution and spreading of the stall vortex over the swept wing is, thus, very different from the evolution, quick growth, and rapid ejection from the surface, observed in the case of two-dimensional flow over an unswept wing. The difference is very striking even when the sweep angle is very small as in the present case.

Conclusions

1) The onset of the dynamic stall vortex in three-dimensional flow over the swept wing is associated with a long pressure plateau (or very mild second suction peak) which replaces the strong second suction peak observed over an unswept wing. Thus, there does not appear to be a rapid ejection/liftoff of the stall vortex from the surface but a rather gradual spreading of the vortex across the wing

surface. This is believed to be due to the occurrence of more gradual, open type, three-dimensional, flow separation in the presence of the spanwise velocity component. Consequently, sweep increases unsteady $C_{l\max}$, as well as the incidence at which it occurs. It causes C_m about the pitching axis to increase at an earlier incidence but less drastically than in two-dimensional flow.

2) The aerodynamic coefficients follow a trend that is an extension of the quasisteady behavior to poststatic stall incidences. This is true at all spanwise locations and at all except the highest pitch rate studied. Of these, the pitching moment coefficient departs the earliest from the quasisteady behavior and shows a large increase well before the occurrence of dynamic stall, whereas the lift and drag coefficients continue to follow a quasisteady trend almost up to the occurrence of dynamic stall. These characteristics are qualitatively similar to those observed in two-dimensional flows.

3) Lift curve slope and maximum lift increase from the bottom toward the top part of the wing. Pitching moment increases in a similar manner, except that the increase begins to appear earlier during the pitching maneuver. The pressure-minimum wave front (usually associated with the stall vortex) convects obliquely along the wing surface from the bottom toward the top of the wing with a longitudinal convection velocity of about $0.17U_0$. All of these effects can be related to the pitch-axis geometry studied in the present experiments.

4) There is strong evidence of spanwise modulation in the production of vorticity at the wing surface, especially in the downstream regions of the wing. In fact, some spanwise modulation can be observed even in the lift distribution. The precise cause of this periodicity is unknown. This aspect requires further study.

Acknowledgment

This work was supported by the U.S. Airforce Office of Scientific Research through Grant F49620-92-J-0146. This support is gratefully acknowledged.

References

[1]Ashworth, J., and Luttges, M., "Comparisons in Three-Dimensionality in the Unsteady Flows Elicited by Straight and Swept Wings," AIAA Paper 86-2280-CP, Aug. 1986.

[2]Robinson, M. C., and Wissler, J. B., "Unsteady Surface Measurements on a Pitching Rectangular Wing," AIAA Paper 88-0328, Jan. 1988.

[3]Robinson, M. C., and Wissler, J. B., "Pitch Rate and Reynolds Number Effects on a Pitching Rectangular Wing," AIAA Paper 88-2577, June 1988.

[4]Lorber, P. F., Carta, F. O., and Covino, A. F., Jr., "An Oscillating Three-Dimensional Wing Experiment: Compressibility, Sweep, Rate, Waveform, and Geometry Effects on Unsteady Separation and Dynamic Stall," United Technologies Research Center, UTRC Rept. R92-958325-6, East Hartford, CT, Nov. 1992.

[5]Lorber, P. F., Covino, A. F., Jr., and Carta, F. O., "Dynamic Stall Experiments on a Swept Three-Dimensional Wing in Compressible Flow," AIAA Paper 91-1795, June 1991.

[6]Lorber, P. F., "Tip Vortex, Stall Vortex and Separation Observations on Pitching Three-Dimensional Wings," AIAA Paper 93-2972, July 1993.

[7]McAlister, K. W., and Takahashi, R. K., "NACA 0015 Wing Pressure and Trailing Vortex Measurements," NASA TP 3151, NASA Ames Research Center, Moffett Field, CA, Nov. 1991.

[8]Piziali, R., NASA TM 4632, Sept. 1994.

[9]Zheng, Y., and Ramaprian, B. R., "LDV Measurements in the Three-Dimensional Near Wake of a Stationary and Oscillating Wing," AIAA Paper 92-2689, June 1992.

[10]Szafruga, J., and Ramaprian, B. R., "Pressure Measurements Over the Tip Region of a Rectangular Wing. Part II: Oscillating Wing," AIAA Paper 94-1949, June 1994.

[11]Conger, R. N., and Ramaprian, B. R., "Pressure Measurements on a Pitching Airfoil in a Water Channel," *AIAA Journal*, Vol. 32, No. 1, 1994, pp. 108–115.

[12]Conger, R. N., and Ramaprian, B. R., "The WSU-MME 1 m × 0.7 m Water Channel," Mechanical and Materials Engineering Dept., Rept. MME-TF-92-1, Washington State Univ., Pullman, WA, May 1992.

[13]Conger, R. N., and Ramaprian, B. R., "Correcting for Response Lag in Unsteady Pressure Measurements in Water," *Journal of Fluids Engineering*, Vol. 115, Dec. 1993, pp. 676–679.

[14]Patterson, A., "Surface Pressure Measurements on a Pitching Swept Airfoil in a Water Channel," M.S. Thesis, Mechanical Materials Engineering. Dept., Washington State Univ., Pullman, WA, Dec. 1933.

[15]Rymarz, P. B., "Measurements of Velocity and Vorticity Fields around a Pitching Swept Wing," M.S. Thesis, Dept. of Mechanical and Materials Engineering, Washington State Univ., Pullman, WA, May 1955.

[16]Green, R. B., Galbraith, R. A. McD., and Niven, A. J., "Measurement of the Dynamic Stall Vortex Convection Speed," *Aeronautical Journal*, Vol. 96, Oct. 1992, pp. 319–325.

[17]Wang, K. C., "Separation Patterns of Boundary Layer Over an Inclined Body of Revolution," *AIAA Journal*, Vol. 10, No. 8, 1972, pp. 1044–1050.

[18]Panton, R. L., *Incompressible Flow*, Wiley, New York, 1984, Chap. 13.